Sodium channel β1 subunits are post-translationally modified by tyrosine phosphorylation, S-palmitoylation, and regulated intramembrane proteolysis

Alexandra A. Bouza[1,‡], Julie M. Philippe[1,‡], Nnamdi Edokobi[1], Alexa M. Pinsky[1], James Offord[1], Jeffrey D. Calhoun[1], Mariana Lopez-Florán[1], Luis F. Lopez-Santiago[1], Paul M. Jenkins[1,2], and Lori L. Isom[1,3,4,*]

From the Departments of [1]Pharmacology, [2]Psychiatry, [3]Molecular and Integrative Physiology, and [4]Neurology, University of Michigan Medical School, Ann Arbor, Michigan, USA

Edited by Mike Shipston

Voltage-gated sodium channel (VGSC) β1 subunits are multifunctional proteins that modulate the biophysical properties and cell-surface localization of VGSC α subunits and participate in cell–cell and cell–matrix adhesion, all with important implications for intracellular signal transduction, cell migration, and differentiation. Human loss-of-function variants in *SCN1B*, the gene encoding the VGSC β1 subunits, are linked to severe diseases with high risk for sudden death, including epileptic encephalopathy and cardiac arrhythmia. We showed previously that β1 subunits are post-translationally modified by tyrosine phosphorylation. We also showed that β1 subunits undergo regulated intramembrane proteolysis via the activity of β-secretase 1 and γ-secretase, resulting in the generation of a soluble intracellular domain, β1-ICD, which modulates transcription. Here, we report that β1 subunits are phosphorylated by FYN kinase. Moreover, we show that β1 subunits are S-palmitoylated. Substitution of a single residue in β1, Cys-162, to alanine prevented palmitoylation, reduced the level of β1 polypeptides at the plasma membrane, and reduced the extent of β1-regulated intramembrane proteolysis, suggesting that the plasma membrane is the site of β1 proteolytic processing. Treatment with the clathrin-mediated endocytosis inhibitor, Dyngo-4a, restored the plasma membrane association of β1-p.C162A to WT levels. Despite these observations, palmitoylation-null β1-p.C162A modulated sodium current and sorted to detergent-resistant membrane fractions normally. This is the first demonstration of S-palmitoylation of a VGSC β subunit, establishing precedence for this post-translational modification as a regulatory mechanism in this protein family.

Voltage-gated sodium channels (VGSCs) are heterotrimeric protein complexes composed of one pore-forming α subunit and two non–pore-forming β subunits (1). VGSC β1–β4 subunits contain a single, extracellular V-type immunoglobulin (Ig) domain and are thus members of the Ig superfamily of cell adhesion molecules (Ig-CAMs) (1, 2). β1 subunits are expressed in multiple tissues, including brain and heart, where they modulate the gating, kinetics, and plasma membrane localization of

VGSC α subunits through noncovalent association (2–5). β1 subunits are multifunctional and play both conducting and nonconducting roles. In addition to modulating VGSCs, they contribute to voltage-gated potassium channel function, cell–cell and cell–matrix adhesion and cell migration, intracellular calcium signaling, neuronal pathfinding and fasciculation, neurite outgrowth, and cardiac intercalated disk formation (2, 6–13). Concordant with their CAM function, β1–β1 *trans*-homophilic cell adhesion *in vitro* results in outside-in signaling that includes ankyrin recruitment to points of cell–cell contact, which is terminated by β1 tyrosine phosphorylation (9, 10). In cultured cerebellar granule neurons, β1–β1 *trans*-homophilic cell adhesion drives neurite extension through a mechanism that includes *fyn* kinase (8). β1 subunits form heterophilic partnerships with other CAMs, including contactin, N-cadherin, NrCAM, neurofascin, and VGSC β2 subunits, and associate with the extracellular matrix protein tenascin-R to modulate cell migration (14–16). Thus, β1 CAM activity is critical for brain and heart development.

Human variants in VGSC genes are linked to the developmental and epileptic encephalopathies (DEEs) and to cardiac arrhythmia. Loss-of-function variants in *SCN1B*, encoding β1, result in early infantile developmental and epileptic encephalopathy (EI-DEE) and generalized epilepsy with febrile seizures plus (2, 17). *Scn1b*-null mice model EI-DEE, with severe spontaneous seizures of multiple etiologies, ataxia and sudden death in the third week of life (18). Consistent with loss of β1-mediated cell–cell and cell–matrix adhesion, *Scn1b*-null mice have neuronal pathfinding and fasciculation defects in the brain (6, 8). *SCN1B* is expressed in the heart in addition to the brain. *Scn1b*-null mice have prolonged QT and RR intervals. *Scn1b*-null ventricular cardiomyocytes have increased sodium current (I_{Na}), altered calcium handling, altered intercalated disk structure, and prolonged action potential duration (13, 19, 20). *SCN1B* variants are associated with human cardiac disease, including Brugada syndrome and atrial fibrillation (21–25). Taken together, these data show that *SCN1B* is critical for the regulation of excitability in multiple organ systems.

β1 subunits undergo regulated intramembrane proteolysis (RIP) through the sequential activity of β-site amyloid precursor protein (APP) cleaving enzyme-1 (BACE1) and

γ-secretase (26).[5] BACE1 cleavage, the rate-limiting step in this process, releases the extracellular β1 Ig domain, which functions as a CAM ligand to stimulate neurite outgrowth (28, 29). The remaining membrane-bound C-terminal fragment (β1-CTF) is cleaved by γ-secretase in the lumen of the membrane, generating a soluble, intracellular domain, β1-ICD, that translocates to the nucleus to regulate transcription (26, 30). Thus, β1 RIP plays important roles in neurite outgrowth, cell migration, cell adhesion, and transcription (31, 32).

BACE1- and γ-secretase–mediated processing of the well-studied RIP substrate, APP, is regulated by *S*-palmitoylation, the covalent addition of a 16-carbon fatty acid to cysteine residues via thioester bond formation (33). Palmitoylation targets APP to its proper membrane domains, bringing it in close proximity to proteolytic enzymes for subsequent cleavage (33). Here, we asked whether post-translational modification of β1 subunits by tyrosine phosphorylation or *S*-palmitoylation could regulate its plasma membrane localization and subsequent RIP. In contrast to β1-ankyrin association, for which β1 tyrosine phosphorylation is critical (10), we found that the tyrosine phosphorylation state of β1 has no effect on its plasma membrane localization, intramembrane cleavage, or ability to modulate I_{Na}. We report for the first time that β1 subunits are *S*-palmitoylated in mouse brain. Using heterologous cells, we found that substitution of cysteine residue 162 with alanine abolishes β1 palmitoylation, decreases the fraction of β1 in the plasma membrane as assessed by surface biotinylation, and thus reduces the level of β1 that is available for RIP. Treatment of cells with the clathrin-mediated endocytosis inhibitor, Dyngo-4a, restores β1-p.C162A to WT levels at the plasma membrane, suggesting that *S*-palmitoylation confers plasma membrane stability to β1. Finally, we show that β1-mediated modulation of I_{Na} and β1 sorting to detergent-resistant membrane fractions do not depend on β1 palmitoylation. Taken together, our work suggests that multiple post-translational modification events regulate β1 function. Tyrosine phosphorylation regulates the association of β1 subunits with ankyrin but does not affect their plasma membrane localization. In contrast, *S*-palmitoylation regulates the cell-surface localization of β1 and consequently its extent of RIP, indicating that β1 cleavage occurs at the plasma membrane. This work provides novel insights into β1 subunit function that may aid in understanding the mechanism of *SCN1B*-associated pathophysiologies.

Results

β1 RIP occurs independently of β1 tyrosine phosphorylation

β1 tyrosine residue 181, located in the intracellular domain, is important for β1-mediated downstream signaling (10) (Fig. 1*A*). In previous work, we used phosphorylation-null and phosphomimetic mutant constructs to show that phosphorylation of residue Tyr-181 is a key regulatory mechanism for ankyrin binding (10). Our work in cerebellar granule neurons demonstrated that β1–β1 *trans*-homophilic adhesion–mediated neurite outgrowth is inhibited by the admin-

istration of γ-secretase inhibitors and in neurons isolated from *fyn*-null mice (8, 31). Taken together, these data suggested that β1-mediated neurite outgrowth requires association of the β1 intracellular domain with ankyrin via residue Tyr-181, which then triggers β1 RIP. Here, we tested the hypothesis that β1 tyrosine phosphorylation regulates cleavage using a multidisciplinary approach.

We used a cell-free fyn kinase assay (Promega) in which ADP was measured via luciferase activity and positively correlated to kinase activity to determine whether fyn directly phosphorylates a β1 peptide, QENASEYLAITC, at position Tyr-7, which is equivalent to position Tyr-181 in the full-length polypeptide. Poly-E_4Y_1 peptide was used as a positive control for fyn kinase activity (Fig. 1*B*). Inclusion of WT β1 peptide in the assay increased luciferase activity by ~3-fold over the no-substrate control. In contrast, luciferase activity levels in the presence of Y181E β1 peptide (pYβ1) were not different from the no-substrate control. These data indicate that fyn kinase can directly phosphorylate β1 at the Tyr-181 position (Fig. 1*B*).

To understand whether β1 phosphorylation at Tyr-181 affects β1 RIP, we generated phosphorylation-null, β1-p.Y181A-V5-2A-eGFP, and phosphomimetic, β1-p.Y181E-V5-2A-eGFP mutant constructs, based on our previous work (10). Chinese hamster lung (CHL) cell lines stably overexpressing each construct were generated, and plasma membrane localization of each mutant polypeptide was investigated using cell-surface biotinylation assays (29, 30). Similar to WT β1, both β1 mutants were detected in the plasma membrane fraction (Fig. 1*C*). Quantification of these results showed no differences in the plasma membrane association of any of the mutants compared with WT β1 (Fig. 1*D*). To determine whether β1 phosphorylation at residue Tyr-181 regulates BACE1- and γ-secretase–mediated cleavage of β1, each cell line was treated with vehicle (0.1% DMSO) or 1 μM of the γ-secretase inhibitor DAPT and analyzed by Western blotting. Treatment with DAPT leads to an accumulation of the intermediary cleavage product, β1-CTF, generated by BACE1 cleavage.[1] We found that levels of β1-CTF were generated similarly to WT in both mutant lines and accumulated similarly to WT following treatment with DAPT, suggesting that neither BACE1 nor γ-secretase cleavage of β1 depends on its phosphorylation state (Fig. 1, *E* and *F*). β1-CTF fragments generated from DAPT treatment of β1 phosphorylation mutants had variable molecular masses, compared with WT β1-CTF. This effect may be similar to previously observed shifting of the cleavage site resulting from the introduction of mutations into other BACE1 substrates (34) and warrants future investigation. These results also suggest that our previous work, demonstrating that γ-secretase inhibitors block β1-mediated neurite outgrowth (31), may have implicated γ-secretase substrates other than β1.

β1 modulation of I_{Na} occurs independently of β1 tyrosine phosphorylation

We next asked whether the phosphorylation state of residue Tyr-181 affects the ability of β1 to modulate I_{Na}. Human Embryonic Kidney (HEK) cells stably expressing human Na$_v$1.5
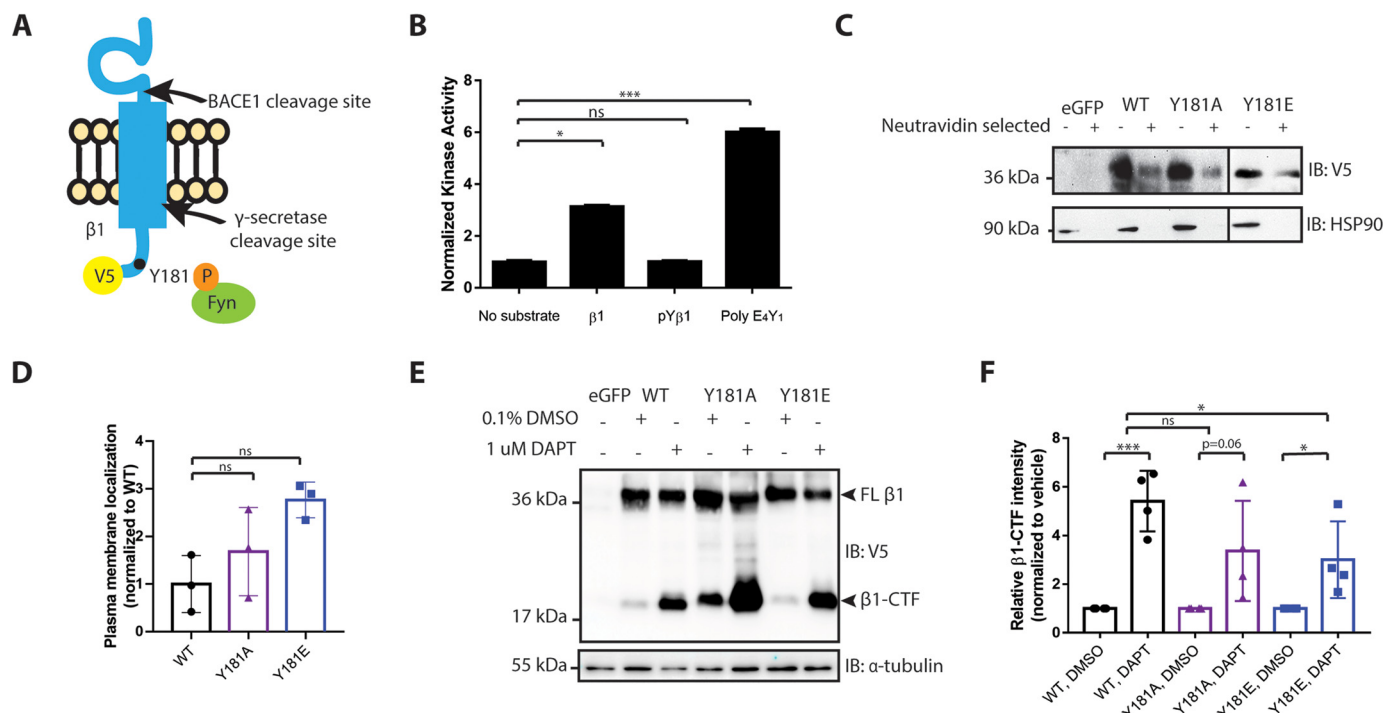
⧟ASBMB

J. Biol. Chem. (2020) 295(30) 10380–10393 **10381**

Figure 1. β1 phosphorylation at residue Tyr-181 does not affect its RIP. *A*, schematic of β1 identifying the location of the phosphorylation site, Tyr-181, as well as BACE1 and γ-secretase cleavage sites. *B*, a β1 peptide (QENASEYLAITC) is directly phosphorylated at Tyr-181 (Tyr-7 in the peptide) by fyn kinase in a cell-free assay ($n = 3$). *C*, cell surface biotinylation indicates that similar to WT β1-V5, β1-p.Y181A-V5, and β1-p.Y181E-V5 are localized to the plasma membrane ($n = 3$). *D*, quantification of *C*. Plasma membrane fraction was normalized to total protein for that construct (% plasma membrane/total) and normalized again to WT β1-V5 plasma membrane levels. Significance ($p < 0.05$) was determined using a one-way ANOVA. *E*, WT β1-V5, β1-p.Y181A-V5, and β1-p.Y181E-V5 are cleaved by BACE1 and γ-secretase ($n = 4$). *F*, quantification of *E*. Protein levels were normalized to the loading control and reported as fold change respective to the vehicle-treated group. Significance ($p < 0.05$) was determined using Student's *t* test between DMSO- and DAPT-treated constructs. One-way ANOVA was utilized to compare between constructs. *IB*, immunoblotting; *ns*, not significant.

(HEK-hNav1.5) were transiently transfected with soluble eGFP, WT β1-V5-2A-eGFP, β1-p.Y181A-V5-2A-eGFP, or β1-p.Y181E-V5-2A-eGFP. Inclusion of eGFP facilitated the identification of transfected cells for whole-cell voltage patch-clamp recordings. Co-expression of WT β1-V5-2A-eGFP, β1-p.Y181A-V5-2A-eGFP, or β1-p.Y181E-V5-2A-eGFP with hNa$_v$1.5 increased I_{Na} density compared with eGFP alone, suggesting that the phosphorylation state of residue Tyr-181 does not affect the ability of β1 to modulate I_{Na} density (Fig. 2, *A* and *B*). In agreement with the observed increase in peak I_{Na} density, peak conductance was increased by co-expression of WTβ1-V5-2A-eGFP, β1-p.Y181A-V5-2A-eGFP, or β1-p.Y181E-V5-2A-eGFP (Fig. 2*C*). No changes in capacitance were observed (Fig. 2*D*). We observed no effects of any of the β1 constructs on the voltage dependence of I_{Na} activation or inactivation compared with the eGFP control (Table S1).

β1 is S-palmitoylated in vitro and in vivo

APP is a type I transmembrane topology BACE1 substrate that results in the generation of Aβ peptides to form protein aggregates that can contribute to Alzheimer's disease pathogenesis (35). BACE1-mediated cleavage of APP is highly dependent on its proper localization in lipid raft microdomains (33). The post-translational lipid modification, *S*-palmitoylation, is required for proper targeting of APP to lipid rafts (33). In lipid rafts, palmitoylated APP interacts with BACE1 for subsequent

cleavage (33). Given its similarity to APP, we asked whether β1 is also *S*-palmitoylated and, if so, whether *S*-palmitoylation regulates β1 subcellular localization and RIP. To assess steady-state palmitoylation of β1, we used the acyl resin-assisted capture (RAC) assay, in which free cysteines are first blocked with the alkylating reagent methyl methanethiosulfonate (MMTS). Then thioester bonds between the cysteine residue of the protein and the palmitate are cleaved using the reducing agent hydroxylamine (HA/NH$_2$OH) to liberate the previously palmitoylated cysteine residues. The liberated cysteines are selectively captured on activated thiol-Sepharose beads and eluted, allowing for specific immunoblotting of palmitoylated proteins of interest (36). We used endogenous flotillin-1, a known constitutively palmitoylated protein (37), as a positive control for the acyl RAC assay. In cells stably expressing WT β1-V5-2A-eGFP, we observed that β1 is *S*-palmitoylated, as evidenced by hydroxylamine-dependent binding of β1-V5 to Sepharose beads (Fig. 3*A* and Fig. S1).

We next asked whether β1 palmitoylation occurs *in vivo*. Using C57Bl/6J adult mouse whole-brain lysates subjected to acyl RAC, we observed β1 palmitoylation, as evidenced by hydroxylamine-dependent binding of endogenous β1 to Sepharose beads (Fig. 3*B*). These data demonstrate that β1 is *S*-palmitoylated *in vitro*, as well as in mouse brain, providing feasibility for investigating the role of *S*-palmitoylation in β1 localization and proteolytic processing.
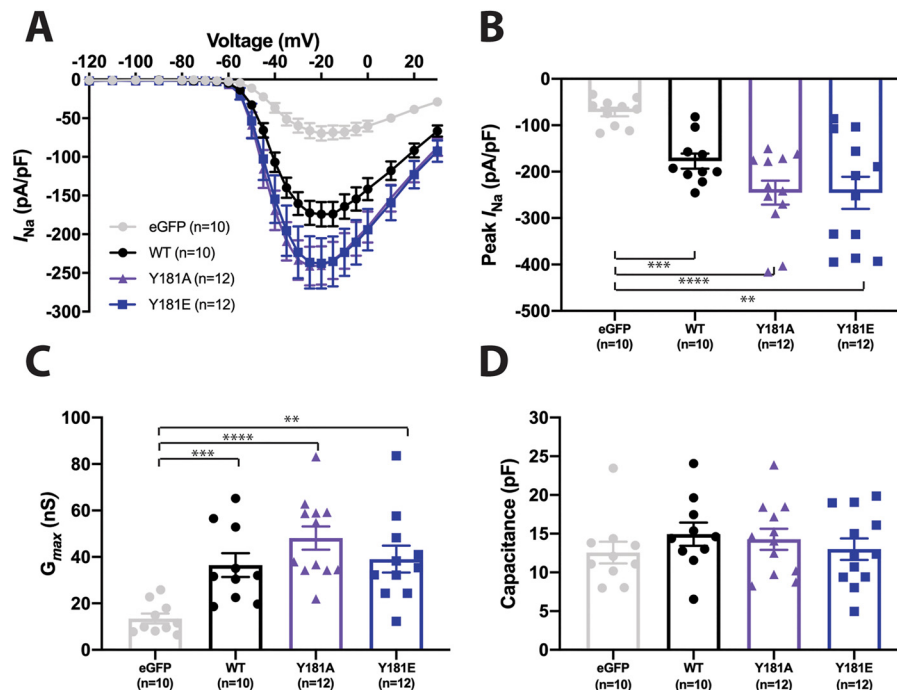
Figure 2. β1-Mediated modulation of I_{Na} is not dependent on phosphorylation of residue Tyr[181]. HEK-hNa$_v$1.5 cells were transiently co-transfected with WTβ1 (*black circles*), β1-p.Y181E (*blue squares*), or β1-p.Y181A (*purple triangles*). HEKhNa$_v$1.5 cells transfected with eGFP (*light gray circles*) were used as negative controls. I_{Na} was recorded in response to a series of voltage steps between −120 and +30 mV in 5-mV increments, from a holding potential of −120 mV for 200 ms. *A*, I_{Na} current–voltage (*I–V*) relationship. *B*, peak I_{Na} is significantly increased with co-expression of WTβ1, β1-p.Y181E, or β1-p.Y181A over eGFP. *C*, peak conductance (G_{max}) is significantly increased with co-expression of WTβ1, β1-p.Y181E, or β1-p.Y181A over eGFP. The data were obtained by fitting individual activation or inactivation curves to a Boltzmann equation. G_{Na} was calculated from $G_{Na} = I_{Na}/(V − V_{rev})$, where I_{Na} is the peak I_{Na} during the test depolarization (*V*), and V_{rev} is the reversal potential. *D*, there were no significant differences in capacitance (in pF) measured from each cell. The data were acquired using pClamp 11 (Molecular Devices) software. The data presented in *A–C* result from at least three separate transfections and are presented as means ± S.E. **, $p < 0.01$ *versus* eGFP; ***, $p < 0.001$ *versus* eGFP; ****, $p < 0.0001$ *versus* eGFP.
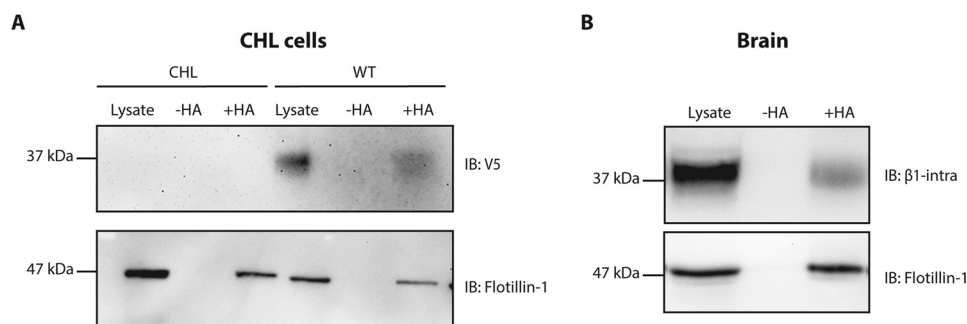

Figure 3. β1 is *S*-palmitoylated in CHL cells and in mouse brain. *A*, CHL cells stably expressing β1-V5-2A-eGFP were processed for the acyl RAC assay to detect *S*-palmitoylation. *S*-Palmitoylation of β1-V5 is detected in CHL cells, as shown by the anti-V5 signal in the +*HA lanes*, compared with the expected absence of signal in the −*HA lanes*. Flotillin-1 is used as a positive control for the acyl RAC assay (*n* = 3). *B*, whole mouse brain lysates were subjected to the acyl RAC assay to detect *S*-palmitoylation. *S*-Palmitoylation of endogenous β1 is detected in whole mouse brains, using an antibody against the C terminus of β1, as shown by the anti-β1 signal in the +*HA lanes*, compared with the expected absence of signal in the −*HA lanes* (*n* = 3). *IB*, immunoblotting.

β1 is S-palmitoylated at cysteine residue 162

To identify the palmitoylated cysteine residue(s) in β1, we first determined the number of palmitoylated sites on β1 using a mass-tag labeling technique, acyl polyethylene glycol (acyl PEG) exchange. In this assay, free cysteine residues are blocked with the alkylating reagent, *N*-ethylmaleimide. Palmitate groups linked to cysteine residues are subsequently cleaved with hydroxylamine and replaced with a 10-kDa PEG-maleimide group, resulting in a 10-kDa shift in the apparent molecular mass of the polypeptide for each palmitoylated cysteine residue, as detected by Western blotting (38). CHL cells stably

expressing WT β1-V5-2A-eGFP were subjected to acyl PEG exchange. We observed a single 10-kDa shift in the apparent molecular mass of β1-V5, which occurred in a hydroxylamine-specific manner, suggesting that β1 is singly palmitoylated (Fig. 4A and Fig. S2). Based on homology models with the CAM myelin P0, which is *S*-palmitoylated at cysteine 153, we predicted that β1 would be palmitoylated at the homologous residue, cysteine 162 (39). Using site-directed mutagenesis, we engineered a cDNA construct in which β1 cysteine residue 162 was converted to an alanine and generated a stable β1-p. C162A-V5-2A-eGFP CHL cell line. To test the effects of

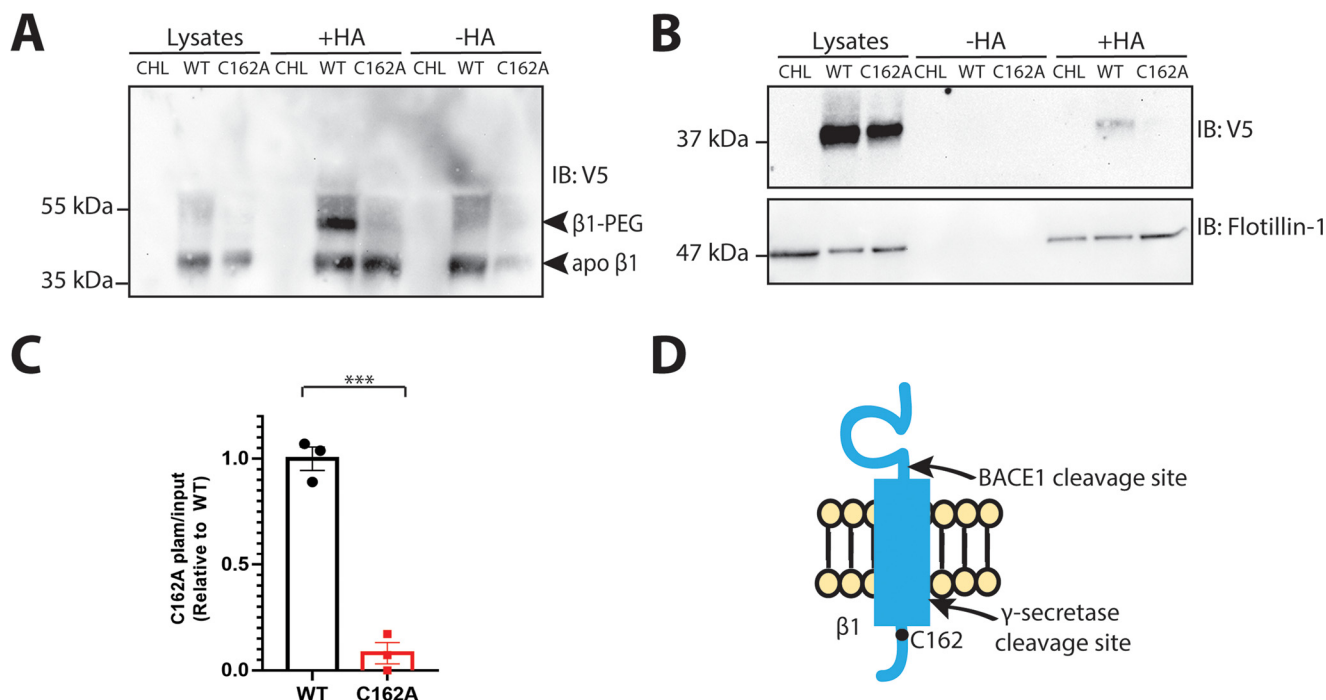**Figure 4. β1 is *S*-palmitoylated at cysteine 162.** *A*, CHL cells stably expressing β1-V5-2A-eGFP or β1-p.C162A-V5-2A-eGFP were processed for the acyl PEG assay to determine the number of palmitoylated cysteines on β1. A single 10-kDa shift in the apparent molecular mass of β1 was observed in a hydroxylamine-specific manner, using an antibody against V5. Compared with WT β1-V5, β1-p.C162A-V5 showed no hydroxylamine-dependent PEGylation-induced mass shift, suggesting loss of the palmitoylation site upon mutation of cysteine to alanine at β1 residue 162 (*n* = 3). *B*, CHL cells stably expressing β1-p.C162A-V5-2A-eGFP were subjected to the acyl RAC assay to detect the effect of the mutation of β1 *S*-palmitoylation. *S*-Palmitoylation of β1-p.C162A-V5 is not detected in CHL cells using an antibody against V5, as shown by the absence of anti-V5 signal in the *+HA lanes*, compared with WT β1-V5 (*n* = 3). *C*, quantification of *B*. The signal from the *+HA lanes* was normalized to total protein for that construct and normalized again to WT β1-V5 palmitoylation levels. Significance (*p* = 0.0003) was determined using a Student's *t* test. *D*, cartoon diagram of β1 and its identified palmitoylation site. *IB*, immunoblotting.

the C162A mutation on β1 palmitoylation, we subjected β1-p.C162A-V5-2A-eGFP CHL cell lysates to both acyl PEG exchange and acyl RAC. Using acyl PEG exchange showed a hydroxylamine-dependent PEGylation-induced mass shift in WT β1-V5 but not in β1-p.C162A-V5, suggesting that β1-p.C162A-V5 cannot be palmitoylated (Fig. 4*A* and Fig. S2). Fig. 4*A* demonstrates a faint, yet present "apo" β1-p.C162A-V5 signal in the −HA lanes, which represents unmodified polypeptide. The control lane is included to show that any PEGylation-induced mass shift observed in the +HA lanes is hydroxylamine-dependent. In this instance, despite the faint "apo" β1-p.C162A-V5 signal in the −HA lanes, the β1-p.C162A-V5 signal in the lysate lane is comparable with the WT β1-V5 signal in the lysate lane, suggesting that the lack of mass shift observed in the +HA lanes for β1-p.C162A-V5 mutant is not due to the lack of starting material but rather due to the loss of the only palmitoylated cysteine residue in β1. We confirmed these results by subjecting β1-p.C162A-V5-2A-eGFP CHL cell lysates to acyl RAC, in which we observed a 92% reduction in the hydroxylamine-dependent signal for β1-p.C162A-V5, compared with WT β1-V5 (Fig. 4, *B* and *C*). These results demonstrate that β1 is singly palmitoylated at cysteine 162 and that mutating this site to alanine completely abolishes β1 palmitoylation (Fig. 4*D*).

β1 *S*-palmitoylation regulates its plasma membrane localization

We asked whether palmitoylation regulates β1 association with the plasma membrane by comparing β1-p.C162A-V5 to WT β1-V5 in cell surface biotinylation assays. We found the level of β1-p.C162A-V5 polypeptide associated with the plasma membrane to be 77% less than WT (1.00 ± 0.1621 for WT *versus* 0.2271 ± 0.0142 for β1-p.C162A), as indicated by the reduced β1-p.C162A-V5 signal in the neutravidin-selected lane (normalized to total protein expression), compared with WT β1-V5 (Fig. 5, *A* and *B*, and Fig. S3). HSP90 was used as a negative control, as in previous work, to ensure that no intracellular biotinylation is occurring (40, 41). These results suggest that *S*-palmitoylation promotes plasma membrane association of β1.

S-Palmitoylation regulates β1 endocytosis but not sorting into detergent-resistant membranes

Palmitoylation has been shown to regulate the partitioning of certain proteins to cholesterol-rich lipid raft microdomains (42). We asked whether palmitoylation governed the localization of β1 to lipid rafts, similarly to what has been shown previously for APP (33). β1 is known to localize to detergent-resistant membrane (DRM) fractions of mouse brain and primary neuronal cultures (8, 26). To verify the presence of β1 in DRM fractions in CHL cells stably expressing WT β1-V5, we prepared DRMs using density gradient centrifugation and analyzed them by Western blotting using anti-V5 antibody. We found that WT β1-V5 was present in both detergent-insoluble fractions, marked with flotillin-1, and in detergent-soluble fractions, marked with transferrin receptor (TfR), similar to previous results (29) (Fig. 6*A*). We observed no differences in this distribution for the palmitoylation-null mutant, β1-p.C162A-
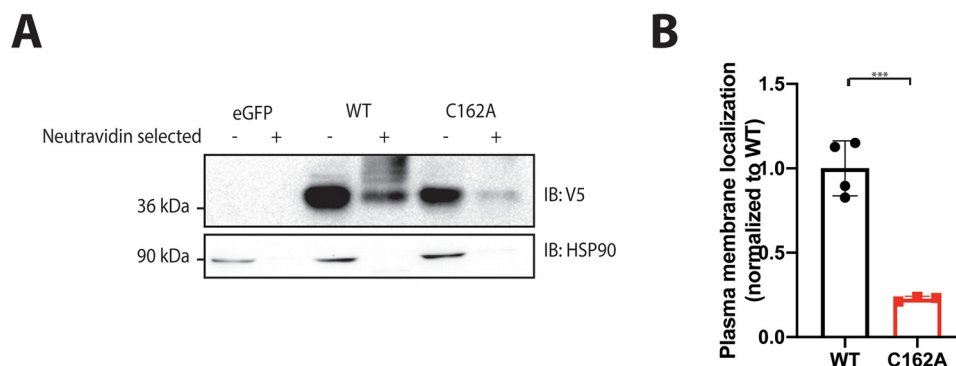
A

B

Figure 5. S-Palmitoylation regulates plasma membrane localization of β1. *A*, CHL cells stably expressing β1-V5-2A-eGFP or β1-p.C162A-V5-2A-eGFP were processed for cell surface biotinylation assay. The level of β1-p.C162A-V5 protein in the biotinylated plasma membrane fraction was reduced compared with WT β1-V5, as evidenced by the lower anti-V5 signal in the neutravidin-selected lane. Soluble HSP90 was used as a negative control (*n* = 3–4). *B*, quantification of *A*. Quantification represents the amount of β1 at the membrane/total β1 protein expression, normalized to WT plasma membrane levels, to obtain a percent reduction in plasma membrane localization in the mutant relative to WT β1 (*n* = 3–4 for each construct). Significance was determined using Student's *t* test.
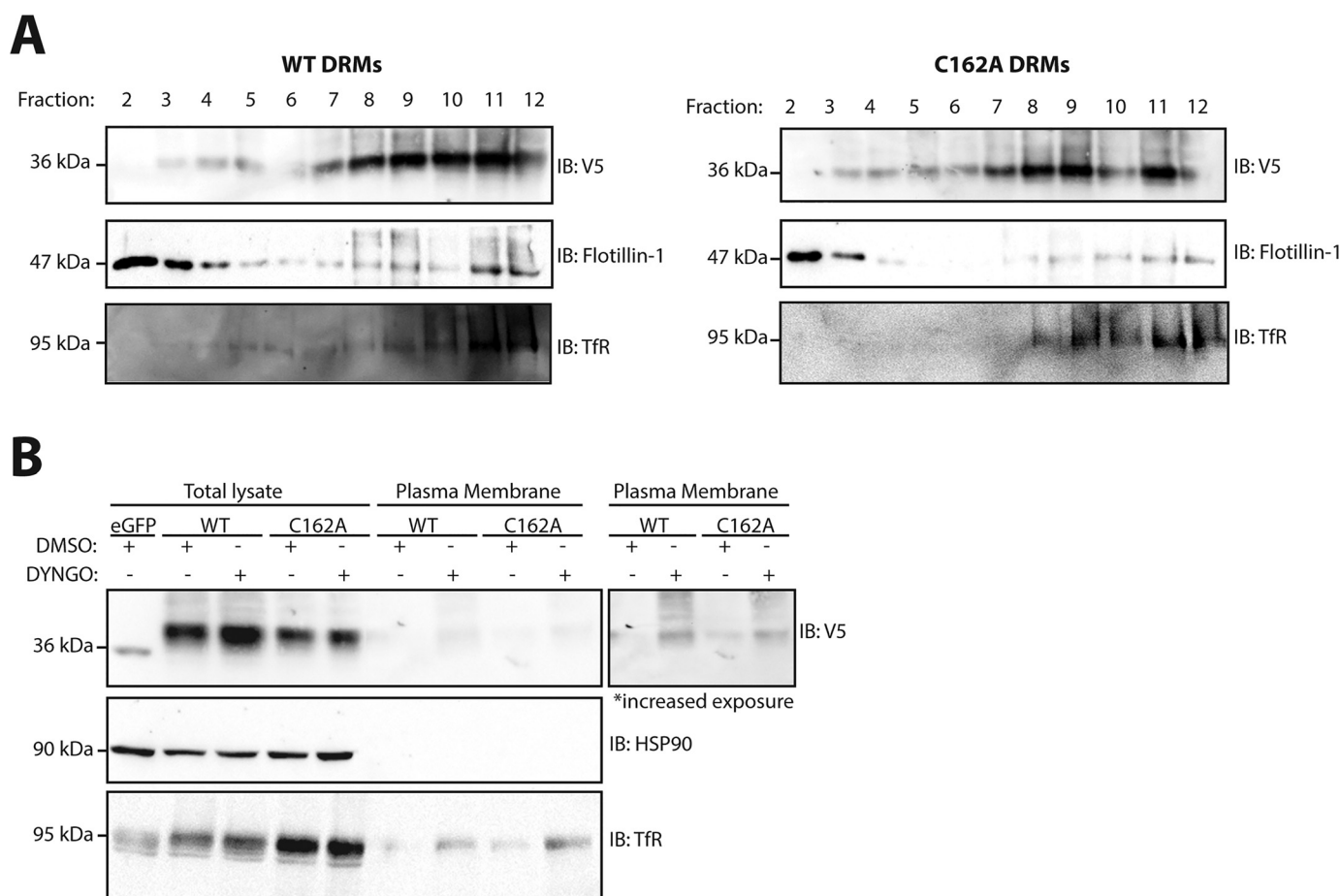
A

B

Figure 6. S-Palmitoylation regulates β1 endocytosis but not sorting into detergent-resistant membranes. *A*, CHL cells stably expressing β1-V5-2A-eGFP or β1-p.C162A-V5-2A-eGFP were processed for discontinuous flotation density gradients to investigate the role of palmitoylation in detergent-resistant membrane partitioning of β1. β1-p.C162A-V5 did not partition differently than WT β1-V5. Flotillin-1 was used as a marker for lipid rafts, whereas TfR was used as a marker for nonraft domains (*n* = 3). *B*, CHL cells stably expressing β1-V5-2A-eGFP or β1-p.C162A-V5-2A-eGFP were treated with vehicle (0.1% DMSO) or 1 μM Dyngo-4a and assessed by cell surface biotinylation. Dyngo-4a treatment restores the plasma membrane level of β1-p.C162A-V5 to that of WT β1 (*n* = 3). *IB*, immunoblotting.

V5, as evidenced by the presence of anti-V5 signal in both flotillin-1-marked DRMs and TfR–marked nonlipid raft domains ([Fig. 6*A*]). These data suggest that although palmitoylation of β1 is necessary for its proper association with the plasma membrane, it does not regulate the partitioning of β1 into lipid-raft domains.

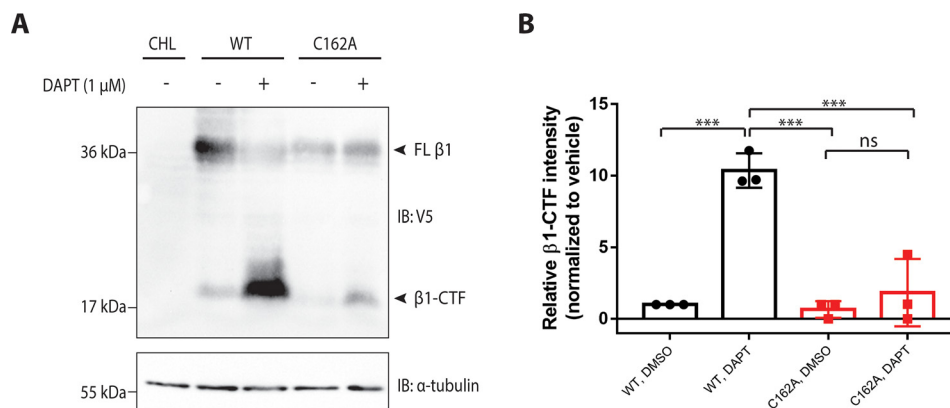Because of the observed reduction of β1-p.C162A at the plasma membrane, we compared the extent of WT β1 *versus*

ASBMB

J. Biol. Chem. (2020) 295(30) 10380–10393 **10385**

A

B

Figure 7. The absence of β1 *S*-palmitoylation at cysteine 162 reduces its level of RIP. *A*, CHL cells stably expressing β1-V5-2A-eGFP or β1-p.C162A-V5-2A-eGFP were treated with vehicle (0.1% DMSO) or 1 μM DAPT. The lysates were subjected to Western blotting analysis to investigate the level of β1 cleavage. Compared with WT β1-V5, β1-p.C162A-V5 shows little to no cleavage product (*n* = 3). *B*, quantification of *A*. Protein levels were normalized to the loading control and reported as fold change respective to the vehicle-treated group. Significance ($p < 0.05$) was determined using one-way ANOVA and plotted as the mean ± S.D. *IB*, immunoblotting; *ns*, not significant.

β1-p.C162A internalization through endocytosis. We treated CHL cells stably expressing β1-V5-2A-eGFP or β1-p.C162A-V5-2A-eGFp with vehicle (0.1% DMSO) or 1 μM of the dynamin inhibitor, Dyngo-4a, and assessed the amount of β1-V5 *versus* β1-p.C162A-V5 accumulation at the cell surface by biotinylation. Anti-HSP90 antibody was used as a negative control for the plasma membrane fraction, and anti-TfR antibody was used as a positive control for endocytosis inhibition with Dyngo-4a. We found that Dyngo-4a administration normalized the level of β1-p.C162A-V5 in the plasma membrane fraction to that of WT β1, implicating clathrin-dependent endocytosis in this process (Fig. 6*B*). Pulldown experiments are inherently variable. This variability accounts for the apparent presence of higher levels of plasma membrane association of β1-p.C162A in the DMSO-treated control samples compared with WT β1 DMSO-treated control samples. It is important to note that, in this particular instance, pulldown was more efficient in the mutant DMSO-treated samples compared with WT, as evident by the higher TfR signal. This work adds new information to the VGSC field, showing that WT β1 subunits undergo endocytosis via a clathrin-dependent mechanism and suggesting that the palmitoylation may confer plasma membrane stability to β1 polypeptides.

The level of β1-p.C162A RIP is reduced compared with WT

We hypothesized that reduction in plasma membrane localization of β1-p.C162A-V5 would reduce its level of RIP. To test this hypothesis, we treated stable β1-V5-2A-eGFP or β1-p.C162A-V5-2A-eGFP CHL cells with vehicle (0.1% DMSO) or 1 μM DAPT and assessed the formation of the ~20-kDa β1 intramembrane CTF by Western blotting analysis. As shown previously, inhibition of γ-secretase by DAPT results in β1-CTF accumulation in the presence of normally occurring BACE1 cleavage.[1] If BACE1-mediated β1 cleavage were altered or reduced, DAPT administration would result in reduced levels of β1-CTF accumulation because of a reduction in available substrate for γ-secretase–mediated RIP. As expected, DAPT treatment of CHL cells stably expressing WT β1-V5 resulted in

β1-CTF accumulation (Fig. 7, *A* and *B*). In contrast, using the β1-p.C162A-V5 mutant construct as substrate resulted in an 80% loss in the level of cleavage product compared with WT (Fig. 7, *A* and *B*). This result suggests that BACE1 cleaves the small fraction of β1-p.C162A-V5 that is localized to the plasma membrane, generating a reduced level of β1-CTF in response to DAPT treatment, compared with WT β1. These data demonstrate that β1 palmitoylation promotes β1 plasma membrane localization, which allows RIP to occur.

β1-mediated modulation of I_{Na} is not affected by palmitoylation

We next asked whether palmitoylation-deficient β1-p.C162A-V5 could modulate I_{Na}. WT β1-V5-2A-eGFP, β1-p.C162A-V5-2A-eGFP, or eGFP were transiently expressed in HEK-hNa$_v$1.5 cells. We found that WT β1-V5 and β1-p.C162A-V5 increased I_{Na} density to a similar extent, compared with the soluble eGFP control (Fig. 8, *A* and *B*). In agreement with the observed increase in peak I_{Na} density, peak conductance was increased by co-expression of WT β1-V5-2A-eGFP or β1-p.C162A-V5-2A-eGFP (Fig. 8*C*). No changes in capacitance were observed (Fig. 8*D*). We observed no effect of either β1 construct on the voltage dependence of I_{Na} activation or inactivation (Table S1). These data suggest that the small fraction of β1-p.C162A-V5 that remains properly localized to the plasma membrane (Fig. 5, *A* and *B*) is sufficient to modulate I_{Na}.

Discussion

VGSC β1 subunits are multifunctional signaling molecules. In addition to modulating the gating, kinetics, and localization of VGSC α subunits, β1 subunits function in cell–cell and cell–matrix adhesion, cell migration, calcium handling, modulation of potassium currents, neuronal pathfinding, fasciculation, and neurite outgrowth (2). Human *SCN1B* loss-of-function variants are linked to EI-DEE and cardiac arrhythmia, often resulting in sudden death (2).

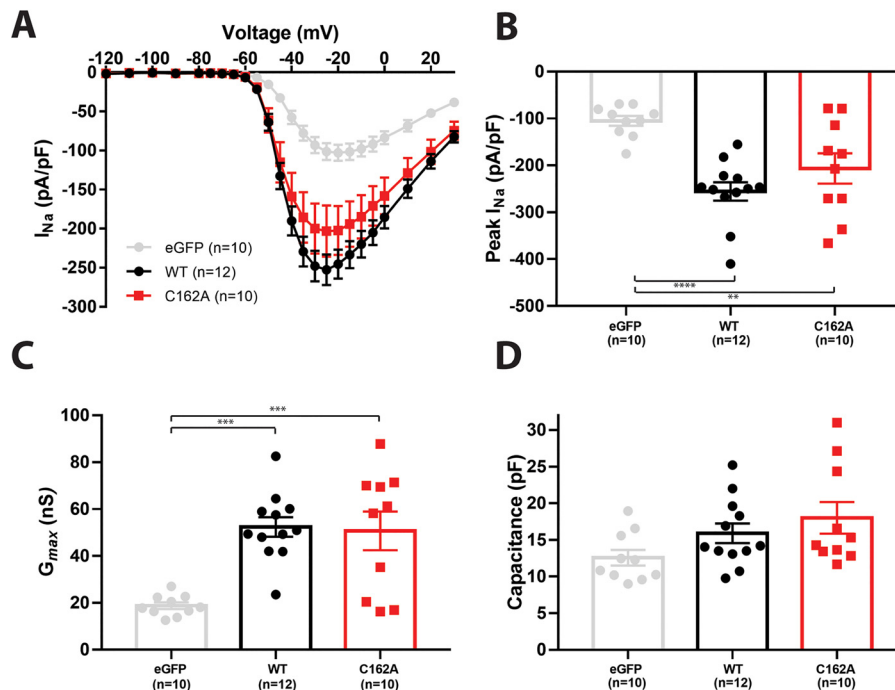It is important to understand how β1 subunits are post-translationally processed and whether this differential

Figure 8. β1-Mediated modulation of I_{Na} density is not dependent on S-palmitoylation of β1 at residue Cys-162. HEK-hNa$_v$1.5 cells were transiently co-transfected with eGFP, WTβ1, or β1-p.C162A. *A*, I_{Na} current–voltage (*I–V*) relationship. *B*, peak I_{Na} is significantly increased with co-expression of WTβ1 or β1-p.C162A over eGFP. *C*, peak conductance (G_{max}) is significantly increased with co-expression of WTβ1 or β1-p.C162A over eGFP. *D*, no significant difference in the capacitance (in pF) measured from each cell. The data presented in *A–C* result from at least three separate transfections and are presented as means ± S.E. *, $p < 0.05$ *versus* eGFP; ***, $p < 0.001$ *versus* eGFP; ****, $p < 0.0001$ *versus* eGFP.

processing affects their functionality. We showed previously that β1 is tyrosine-phosphorylated (10). Here, we extend those findings to show that fyn kinase directly phosphorylates a β1 peptide, supporting our previous, indirect, hypothesis using neurons from *fyn*-null mice (8). β1 subunits undergo RIP through the activity of BACE1 and γ-secretase (26).[1] Initial cleavage of β1 by BACE1 sheds the β1 Ig ectodomain and leaves behind the β1 C-terminal fragment in the membrane, which undergoes subsequent cleavage by γ-secretase to generate a soluble intracellular domain, the β1-ICD (26). Recent work by our laboratory demonstrated that the β1-ICD can translocate to the nucleus, where it participates in transcriptional regulation to ultimately modulate sodium, potassium, and calcium currents in mouse ventricular myocytes (44).[1] Overexpression of the β1-ICD resulted in the down-regulation of genes related to proliferation, immune response, and sodium and potassium channels. In contrast, loss of β1-ICD in *Scn1b*-null mouse cardiac ventricular tissue resulted in the up-regulation of these gene groups, suggesting that the β1-ICD may act as part of a transcriptional repressor complex under normal physiological conditions. Here, we asked whether β1 tyrosine phosphorylation or β1 S-palmitoylation can regulate β1 RIP. Using β1 phosphorylation-null and phosphomimetic mutant constructs, we found that β1 tyrosine phosphorylation at Tyr-181 does not regulate β1 RIP.

Here, we demonstrate that β1 is lipid-modified by S-palmitoylation in the brain, that S-palmitoylation, but not tyrosine phosphorylation, regulates β1 RIP by facilitating β1 localization to the plasma membrane, and that β1 subunits undergo

clathrin-mediated endocytosis, at least in the absence of VGSC α subunits. Our results suggest that β1 must be associated with the plasma membrane for RIP to occur and that S-palmitoylation at residue Cys-162 stabilizes β1 plasma membrane association and reduces its level of endocytosis. Given that S-palmitoylation has been shown to contribute to protein stability in other work (34), it is possible that reduction of palmitoylation-null β1-C162A protein expression compared with WT β1 is due to decreased β1 protein stability. It will be important to test this hypothesis in follow-up studies. Residue Cys-162, at which β1 is palmitoylated, is conserved in VGSC β3 subunits and thus may implicate palmitoylation as a similar regulatory mechanism in these proteins. The absence of this conserved residue in VGSC β2 and β4 suggests alternative regulatory mechanisms (Fig. S4). Previous work has shown that palmitoylation of APP promotes its RIP through regulating its subcellular localization (33). Although other RIP substrates, *e.g.* LRP1 and N-cadherin, have been shown to be palmitoylated, whether palmitoylation also regulates their RIP is not known (30, 41).

The biochemical experiments described here were performed in the absence of VGSC α subunits. It will be interesting in future work to consider the effects of α subunit co-expression on β1 subunit post-translational processing. Although a large body of work has shown that β1 subunits function as molecular chaperones for VGSC α subunits to the plasma membrane (46), there is no evidence to support the promotion of β1 subunit cell surface expression by α subunits. We do not know whether the reduction in β1-C162A cell surface expression compared with WT β1 shown here could be due to the absence

of a co-expressed α subunit. One possible interpretation of our electrophysiological data showing that $\beta1$-C162A increases I_{Na} density similar to WT is that the presence of an α subunit changes the behavior of this mutant, resulting in intersubunit, synergistic effects. Biochemical assessment of whether α subunits can promote $\beta1$ cell surface expression would be complicated by the noncovalent association of these subunits. Noncovalent α–$\beta1$ association precludes separation of the pool of $\beta1$ subunits associated with α from those that are not, using standard immunoprecipitation techniques. Furthermore, because VGSC α and $\beta1$ subunits are each ankyrin-binding proteins (9, 10, 49, 50), they may associate in a complex, as assessed by co-immunoprecipitation, but not physically interact. Nevertheless, examining the effects of $\beta1$ palmitoylation and phosphorylation in the presence of VGSC α subunits, both in heterologous systems and within the channelome complex in brain and heart *in vivo*, will be interesting future directions of this work.

The effects of $\beta1$ co-expression on I_{Na} voltage-dependent properties in heterologous systems are inconsistent throughout the literature (46). Here, we show that co-expression of hNa$_v$1.5 with $\beta1$ or the mutant $\beta1$ subunits did not statistically change the voltage dependence of activation or steady-state inactivation compared with α (eGFP) alone. In contrast, we observed increased peak I_{Na} density and peak conductance, in agreement with the well-established role of WT $\beta1$ subunits in increasing VGSC function by increasing their plasma membrane expression (46). Interestingly, co-expression of the Tyr-181 or Cys-162 $\beta1$ mutants resulted in increased peak I_{Na} density and maximal conductance. Finally, although Na$_v$1.5 is the major cardiac VGSC, a sizable body of work in recent years has also identified Na$_v$1.5 in the brain (51–53), suggesting that our results may be applicable to other VGSCs.

Importantly, *Scn1b* deletion in mice and heterologous $\beta1$ expression in cell culture are not comparable. *Scn1b*-null mouse cardiac myocytes have increased I_{Na} density because of developmentally regulated increases in the expression of *Scn3a* and *Scn5a* mRNA and protein (19, 20). As described above, our group has recently shown that $\beta1$ is a substrate for RIP by BACE1 and γ-secretase *in vivo* (44).[1] The cleaved C-terminal fragment of $\beta1$ can translocate to the nucleus, resulting in reduced expression of a number of genes, including ion channels. We have proposed that the absence of $\beta1$ subunits in *Scn1b*-null animals results in the absence of gene repression and subsequent increased ion channel expression. This situation is very different from acute, heterologous overexpression of VGSC $\beta1$ and α subunit cDNAs, in which $\beta1$ subunits function to chaperone α subunits to the plasma membrane, as demonstrated here. The required genetic regulatory elements are not present in the cDNA plasmids. Moreover, whereas $\beta1$-chaperone function is lost in *Scn1b*-null mouse myocytes, I_{Na} reductions are not observed. It is likely that the presence of a host of other protein components of the channel proteome that retain VGSCs in the cardiac myocyte plasma membrane (54).

In conclusion, *S*-palmitoylation is a reversible post-translational modification, making it a highly dynamic and tunable process (27, 43, 45, 55). Multiple palmitoyl acyltransferase enzymes, which mediate substrate palmitoylation, as well as

protein thioesterases, which depalmitoylate substrates, are implicated in this process. The molecular identities of the enzymes that palmitoylate and depalmitoylate $\beta1$ subunits are not known but may be identified in the future to discover novel targets for *SCN1B*-linked pathophysiology. In addition, we do not yet know whether the level of $\beta1$ palmitoylation can be dynamically regulated by extracellular stimuli or by altered excitability, but this information will be important to elucidate because attempts to implicate this post-translational processing in disease mechanisms move forward. It is possible that $\beta1$-mediated transcriptional regulation via RIP can be manipulated by altering the level of $\beta1$ palmitoylation. Additionally, the effects of *SCN1B* disease-linked variants on $\beta1$ subunit palmitoylation, RIP, and transcriptional regulation should be considered.

Experimental procedures

Cell culture

CHL cell lines stably expressing $\beta1$ or $\beta1$ mutants and stable HEK-hNa$_v$1.5 cells were grown in Dulbecco's modified Eagle's medium with 5% heat-inactivated fetal bovine serum, penicillin/streptomycin, and 600 μg/ml at 37℃, 5% CO$_2$. Stable cell lines were generated by transfecting parental CHL cells with 1 μg of cDNA with 5 μl of Lipofectamine 2000. 48 h after transfection, the cells were split into medium containing 600 μg/ml G418 (Gibco). The cells were grown for approximately 1 week or until eGFP-positive colonies were large enough to isolate. Individual colonies were selected and grown until confluent and characterized by Western blotting analysis. Patch-clamp experiments used transient transfection of $\beta1$ cDNAs into stable HEK-hNav1.5 cells. 1 μg of cDNA was transfected with 5 μl of Lipofectamine 2000 (Invitrogen). Approximately 12 h post-transfection, the cells were plated for electrophysiological recordings. Patch clamp was completed ~12 h after final plating.

Antibodies

The primary antibodies used were anti-$\beta1_{intra}$ (1:1000 dilution, Cell Signaling Technology), anti-V5 (1:1000 dilution, Invitrogen), anti–α-tubulin (1:1000 dilution, Cedar Lane), anti-HSP90 (1:1000 dilution, EnzoScientific), anti-TfR (1:1000 dilution, Thermo), and anti–flotillin-1 (1:1000, Cell Signaling Technologies). The specificity of anti-$\beta1_{intra}$ has been shown previously by Western blotting (40). Horseradish peroxidase–conjugated secondary antibodies were used in this study. Goat anti-rabbit or goat anti-mouse horseradish peroxidase–conjugated antibodies were diluted 1:1000 (anti-$\beta1_{intra}$, anti–α-tubulin, and anti-TfR) or 1:10,000 (anti-V5, anti–flotillin-1, and anti-HSP90).

Expression vectors

A synthesis-optimized human WT $\beta1$-V5-2A-eGFP cDNA was generated by gBLOCK from Integrated DNA Technologies based on NP_001028.1. The bicistronic cDNA construct included an in-frame $\beta1$ C-terminal V5 epitope tag followed by a self-cleaving 2A peptide and eGFP to facilitate immune

detection of β1 as well as transfected cells by eGFP. β1-p.C162A-V5-2A-eGFP, β1-p.Y181A-V5-2A-eGFP, and β1-p.Y181E-V5-2A-eGFP were generated by site-directed mutagenesis using the WT β1-V5-2A-eGFP cDNA construct in pENTR-SD/D TOPO as the template. The eGFP alone control was generated by PCR from their respective full-length template cDNAs containing WT β1-V5-2A-eGFP. Using the Gateway cloning system, all constructs were moved from pENTR-SD/D-TOPO to pcDNAdest40 via LR Clonase reaction according to the manufacturers' protocol.

The amino acid numbering scheme for the β1 polypeptides used throughout the paper excludes the N-terminal, 19-amino acid signal peptide, as described in the original report of the β1 cDNA sequence (4).

Animals

The animals were housed in the Unit for Laboratory Animal Medicine at the University of Michigan. All procedures were performed in accordance with National Institutes of Health guidelines with approval from the University of Michigan Institutional Animal Care and Use Committee.

Measurement of I_{Na} by whole-cell voltage clamp

Voltage-clamp recordings were performed at room temperature in the whole-cell configuration using an Axopatch 700B amplifier and pClamp (versions 11, Axon Instruments, Foster City, CA) with 1.5–2.5 MΩ patch pipettes. I_{Na} was recorded in the presence of a bath solution containing 120 mM NaCl, 1 mM BaCl$_2$, 2 mM MgCl$_2$, 0.2 mM CdCl$_2$, 1 mM CaCl$_2$, 10 mM HEPES, 20 mM TEA-Cl, and 10 mM glucose (pH 7.35 with CsOH; osmolarity was 300–305 mOsm). Fire-polished patch pipettes were filled with an internal solution containing 1 mM NaCl, 150 mM *N*-methyl-D-glucamine, 10 mM EGTA, 2 mM MgCl$_2$, 40 mM HEPES, 25 mM phosphocreatine-tris, 2 mM MgATP, 0.02 mM Na$_2$GTP, and 0.1 mM leupectin (pH 7.2 with H$_2$SO$_4$). Sodium current was recorded in response to a series of voltage steps between −100 and +30 mV in 5-mV increments, from a holding potential of −90 mV for 200 ms. A step back to −20 mV for 200 ms was used to determine the voltage dependence of inactivation. Series resistance was compensated 40–65%, and leak subtraction was performed by application of a standard P/4 protocol. Normalized conductance and inactivation curves were generated as described previously (47). Current densities were determined by dividing current amplitude by the cell capacitance (C_m), as determined by application of +10-mV depolarizing test pulses.

Cleavage assays

Stably transfected CHL cells were grown to ∼70% confluence in 100-mm tissue culture plates. The cells were treated with vehicle (0.1% DMSO) or 1 μM DAPT (Cayman Chemical), as indicated in the figure legends. After a 24-h treatment, the cells were harvested, and the membranes were prepared. Briefly, the cell pellets were harvested and resuspended in 50 mM Tris, pH 8.0, with Complete protease inhibitors, EDTA-Free (Roche). On ice, the cells were homogenized 10 times with a Dounce homogenizer followed by sonication. To remove nuclei and insoluble material,

the lysates were spun at 2,537 × *g* for 10 at 4 ℃. The supernatant was removed and spun at 80,000 × *g* for 15 min at 4 ℃. The supernatant was removed, and the membrane-containing pellets were resuspended in 133 μl of 50 mM Tris, pH 8.0, with Complete protease inhibitors, EDTA-Free (Roche) and sonicated on ice to resuspend the membrane-containing pellets. The samples were heated at 85 ℃ for 10 min and separated using 12% SDS-PAGE gels, and Western blots were performed as described below.

Surface biotinylation assays

Stably transfected cells were grown to 90–100% confluence in 100-mm tissue culture plates. Cell surface proteins were biotinylated using a cell surface protein isolation kit (Pierce) following the manufacturer's instructions and as previously described (47). All samples were heated at 85 ℃ for 10 min and separated on 10% SDS-PAGE gels. Western blots were performed as described above. For endocytosis experiments, prior to cell surface biotinylation, the cells were treated with vehicle (0.1% DMSO) or 1 μM Dyngo-4a for two h in a 37℃ incubator with 5% CO$_2$. HSP90 was used as a negative control to detect intracellular biotinylation. Any experiments in which intracellular contamination in the plasma membrane fraction was detected (*e.g.* HSP90 signal in the neutravidin-selected lane) were excluded.

DRM preparations

10–100 mm dishes of CHL cells stably transfected with WT β1-V5-2A-eGFP or p.C162A β1-V5-2A-eGFP were grown to 90–100% confluence. As described previously (48), the cells were washed and resuspended in 2.5 ml of HES buffer (20 mM HEPES, 1 mM EDTA, 250 mM sucrose, pH 7.4) supplemented with 1 mM Na$_3$VO$_4$ and Complete protease inhibitors (Roche). The cells were homogenized by 10 passages through a 22-gauge needle and centrifuged at 245,000 × *g* for 90 min at 4 ℃. The membranes were resuspended with 10 passages through a 22-gauge needle in 2.5 ml of MBS buffer (25 mM MES, 15 mM NaCl, pH 6.5) with 1% Triton X-100 and Complete protease inhibitors (Roche) and incubated for 20 min at 4 ℃. Homogenate was mixed with 2.5 ml of 90% sucrose. 5 ml of 35% sucrose and 2.5 ml of 5% sucrose were overlaid, and the samples were centrifuged at 200,000 × *g* in a swinging bucket rotor for 17 h. 1 ml fractions were collected from top to bottom, heated at 85 ℃ for 10 min with sample buffer, and subsequently analyzed by Western blotting.

Western blotting analysis of cell lysates

Cell lysates were prepared either as described above for cleavage assays, surface biotinylation assays, or DRMs, as appropriate. Loading buffer containing SDS, 5 mM β-mercaptoethanol, and 1% DTT was added to samples and heated for 10 min at 85 ℃. Protein lysates were separated by SDS-PAGE on 10 or 12% Tris-glycine polyacrylamide gels as indicated in the figure legends, transferred to nitrocellulose membrane overnight (16 h, 55 mA, 4 ℃), and probed with antibodies, as indicated in the figure legends. Incubations with anti-V5 or anti-β1$_{intra}$ and their respective secondary antibodies were performed using a SnapID with 10–20-min incubations. Anti–α-tubulin,

anti-$\beta1_{intra}$ anti-TfR, anti–flotillin-1, and anti-HSP90 antibodies were incubated overnight at 4 ℃. Secondary antibodies were incubated for 1 h at room temperature. Immunoreactive bands were detected using West Femto chemiluminescent substrate (GE Health Sciences) and imaged using an iBrightFL1000 (Invitrogen). Blots for each antibody were individually detected within the linear range using the smart exposure feature included in the software package for the Invitrogen iBright imager. Immunoreactive signals from cleavage assays were quantified using ImageJ and normalized to the level of α-tubulin and subsequently to vehicle-treated samples.

Acyl RAC

Stably transfected cells were grown to ~90% confluence in 100-mm tissue culture plates. The cells were lysed in buffer containing 100 mM HEPES, 1 mM EDTA, 2.5% SDS, and 2% MMTS (Sigma), adjusted to pH 7.5, sonicated, and left to rotate at 40 ℃ overnight. Acetone precipitation was performed to remove MMTS: 3× volume of cold acetone were used to precipitate the protein for 20 min at −20 ℃, before spinning down in standard bench-top ultracentrifuge at 5000 × g for 1 min. The supernatant was discarded, and the pellet was washed three times with 70% acetone, each time discarding the supernatant. Protein pellet was left to dry in air and stored overnight at −20 ℃. 12 h later, the protein was resuspended in 500 μl of "binding" buffer containing 100 mM HEPES, 1 mM EDTA, and 1% SDS, adjusted to pH 7.5, sonicated, and vigorously shaken for 1 h, before splitting the protein sample into three 1.5-ml tubes, one with 40 μl for "unmanipulated" starting material and two with 220 μl for the palmitoylation assay (one for +HA and one for −HA condition). A 1:1 slurry of preactivated thiopropyl-Sepharose beads (GE) was prepared using binding buffer (50-mg beads = 250 μl of binding buffer). 50 μl of the activated bead slurry was added to each 220-μl lysate. 50 μl of freshly prepared 2 M HA (Sigma), adjusted to pH 7.5, were then added to the lysate designated "+HA," whereas 50 μl of 2 M NaCl were added to the sample designated "−HA." Hydroxylamine/bead/lysate mixtures were left to incubate at room temperature for 2.5 h, rotating. To wash out the hydroxylamine and NaCl, the beads were spun at 5000 × g for 1 min, and the supernatant was removed and discarded. Bead resin was washed five times with 1 ml of binding buffer, each time spinning at 5000 × g for 1 min and discarding the supernatant to recover the beads. Palmitoylated proteins were eluted using 50 μl of 5× sample buffer supplemented with 100 mM DTT. The samples were heated at 65 ℃ for 10 min, separated on a 10% SDS-PAGE gel, transferred to nitrocellulose, and probed with anti-V5, using anti–flotillin-1 as a positive control.

Acyl PEG exchange

Stably transfected cells were grown to ~90% confluence in 100-mm tissue culture plates. The cells were lysed with blocking buffer consisting of 100 mM HEPES, 150 mM NaCl, 5 mM EDTA, 2.5% SDS, and 200 mM tris(2-carboxyethyl)phosphine (Sigma), adjusted to pH 7.5, sonicated, and rotated at room temperature for 1 h. After 1 h, 12.5 μl of freshly prepared 1 M

N-ethylmaleimide (NEM) (dissolved in ethanol) (Sigma) for 25 mM final NEM concentration were added to each lysate, with rotation overnight at room temperature. To scavenge the NEM, 12.5 μl of 2,3-dimethyl 1,3-butadiene (Sigma) were added to each sample and rotated vigorously for 1 h at room temperature. 100 μl of chloroform were added to each sample, vortexed vigorously for 1 min, and centrifuged at maximum speed for 3 min to achieve phase separation. The supernatant on top of the resulting "protein pancake" was split into three 1.5-ml tubes: one containing 40 μl for "unmanipulated" starting material, one containing 100 μl designed for the +HA condition, and one containing 100 μl designated for the −HA condition. 20 μl of 2 M freshly prepared HA (Sigma), adjusted to pH 7.5, were added to the lysate designated +HA, whereas 20 μl of 2 M NaCl were added to the lysate designated −HA. The HA/lysate mixture was incubated for 2 h at 40 ℃, rotating. The HA and NaCl were desalted using a pre-equilibrated 40K MWCO Zebaspin desalting column (Thermo Fisher). 10 μl of a freshly prepared 20 mM stock of 5-kDa mPEG-maleimide (Sigma) (dissolved in water) were added to each desalted lysate and incubated for 2 h at 40 ℃, rotating. 100 μl of 5 × sample buffer supplemented with 100 mM DTT were added to stop the mPEG-maleimide alkylation reaction and heated for 10 min at 65 ℃. The samples were separated on a 10% SDS-PAGE gel, blotted to nitrocellulose, and probed with anti-V5.

Fyn kinase assay

Fyn kinase assays were performed according to manufacturer's recommendations (Fyn kinase assay kit, Promega). The reactions were performed in triplicate, and each reaction contained 200 ng of active GST-tagged Fyn kinase, 50 μM Ultrapure ATP, 0.2 mg/ml peptide substrate, 50 μM DTT diluted in a standard kinase reaction buffer (contents of 5× buffer: 40 mM Tris, pH 7.5, 20 mM MgCl$_2$, 0.1 mg/ml BSA). β1 peptides corresponded to intracellular domain of β1 surrounding Tyr-181 (amino acids 175–185; β1 peptide, QENASEYLAITC; pYβ1 peptide, QENASEpYLAITC). The poly-E$_4$Y$_1$ peptide is a well-characterized substrate of fyn kinase. Kinase reactions lacking substrate were used to normalize the kinase activity in substrate-containing reactions. Three independent experiments were performed. Statistical significance was determined with Student's t test.

Statistics

Statistical analysis for cleavage assay experiments were completed with n = 3–4 for each experiment. The data are represented as the means ± S.E. β1 mutant cleavage experiments were completed as one-way ANOVA with multiple comparisons to WTβ1 treated with DAPT. For the fyn kinase assay, three independent experiments were performed. Statistical significance was determined with Student's t test. The data are represented as the means ± S.E. Electrophysiology experiments had an n of 10–15 cells/condition for each experiment. The voltage dependence of activation and inactivation were compared using nonlinear fit, maximum current was analyzed using one-way ANOVA with multiple comparisons, and current

density was compared with the control, eGFP, with an unpaired *t* test at each voltage step.

Data availability

All data are contained within the article.

References

1. O'Malley, H. A., and Isom, L. L. (2015) Sodium channel β subunits: emerging targets in channelopathies. *Annu. Rev. Physiol.* **77,** 481–504 CrossRef Medline
2. Bouza, A. A., and Isom, L. L. (2018) Voltage-gated sodium channel β subunits and their related diseases. *Handbook Exp. Pharmacol.* **246,** 423–450 CrossRef Medline
3. Hull, J. M., and Isom, L. L. (2018) Voltage-gated sodium channel β subunits: the power outside the pore in brain development and disease. *Neuropharmacology* **132,** 43–57 CrossRef Medline
4. Isom, L. L., De Jongh, K. S., Patton, D. E., Reber, B. F., Offord, J., Charbonneau, H., Walsh, K., Goldin, A. L., and Catterall, W. A. (1992) Primary structure and functional expression of the β1 subunit of the rat brain sodium channel. *Science* **256,** 839–842 CrossRef Medline
5. Isom, L. L., Ragsdale, D. S., De Jongh, K. S., Westenbroek, R. E., Reber, B. F., Scheuer, T., and Catterall, W. A. (1995) Structure and function of the β2 subunit of brain sodium channels, a transmembrane glycoprotein with a CAM motif. *Cell* **83,** 433–442 CrossRef Medline
6. Brackenbury, W. J., Yuan, Y., O'Malley, H. A., Parent, J. M., and Isom, L. L. (2013) Abnormal neuronal patterning occurs during early postnatal brain development of Scn1b-null mice and precedes hyperexcitability. *Proc. Natl. Acad. Sci. U.S.A.* **110,** 1089–1094 CrossRef Medline
7. Brackenbury, W. J., Calhoun, J. D., Chen, C., Miyazaki, H., Nukina, N., Oyama, F., Ranscht, B., and Isom, L. L. (2010) Functional reciprocity between Na$^+$ channel Nav1.6 and β1 subunits in the coordinated regulation of excitability and neurite outgrowth. *Proc. Natl. Acad. Sci. U.S.A.* **107,** 2283–2288 CrossRef Medline
8. Brackenbury, W. J., Davis, T. H., Chen, C., Slat, E. A., Detrow, M. J., Dickendesher, T. L., Ranscht, B., and Isom, L. L. (2008) Voltage-gated Na$^+$ channel β1 subunit-mediated neurite outgrowth requires Fyn kinase and contributes to postnatal CNS development *in vivo*. *J. Neurosci.* **28,** 3246–3256 CrossRef Medline
9. Malhotra, J. D., Kazen-Gillespie, K., Hortsch, M., and Isom, L. L. (2000) Sodium channel β subunits mediate homophilic cell adhesion and recruit ankyrin to points of cell–cell contact. *J. Biol. Chem.* **275,** 11383–11388 CrossRef Medline
10. Malhotra, J. D., Koopmann, M. C., Kazen-Gillespie, K. A., Fettman, N., Hortsch, M., and Isom, L. L. (2002) Structural requirements for interaction of sodium channel β1 subunits with ankyrin. *J. Biol. Chem.* **277,** 26681–26688 CrossRef Medline
11. Malhotra, J. D., Thyagarajan, V., Chen, C., and Isom, L. L. (2004) Tyrosine-phosphorylated and nonphosphorylated sodium channel β1 subunits are differentially localized in cardiac myocytes. *J. Biol. Chem.* **279,** 40748–40754 CrossRef Medline
12. Marionneau, C., Carrasquillo, Y., Norris, A. J., Townsend, R. R., Isom, L. L., Link, A. J., and Nerbonne, J. M. (2012) The sodium channel accessory subunit Navβ1 regulates neuronal excitability through modulation of repolarizing voltage-gated K$^+$ channels. *J. Neurosci.* **32,** 5716–5727 CrossRef Medline
13. Veeraraghavan, R., Hoeker, G. S., Alvarez-Laviada, A., Hoagland, D., Wan, X., King, D. R., Sanchez-Alonso, J., Chen, C., Jourdan, J., Isom, L. L., Deschenes, I., Smyth, J. W., Gorelik, J., Poelzing, S., and Gourdie, R. G. (2018) The adhesion function of the sodium channel beta subunit (β1) contributes to cardiac action potential propagation. *eLife* **7,** e37610 CrossRef Medline
14. McEwen, D. P., and Isom, L. L. (2004) Heterophilic interactions of sodium channel β1 subunits with axonal and glial cell adhesion molecules. *J. Biol. Chem.* **279,** 52744–52752 CrossRef Medline
15. McEwen, D. P., Meadows, L. S., Chen, C., Thyagarajan, V., and Isom, L. L. (2004) Sodium channel β1 subunit-mediated modulation of Nav1.2 currents and cell surface density is dependent on interactions with contactin and ankyrin. *J. Biol. Chem.* **279,** 16044–16049 CrossRef Medline
16. Xiao, Z. C., Ragsdale, D. S., Malhotra, J. D., Mattei, L. N., Braun, P. E., Schachner, M., and Isom, L. L. (1999) Tenascin-R is a functional modulator of sodium channel β subunits. *J. Biol. Chem.* **274,** 26511–26517 CrossRef Medline
17. Aeby, A., Sculier, C., Bouza, A. A., Askar, B., Lederer, D., Schoonjans, A.-S., Vander Ghinst, M., Ceulemans, B., Offord, J., Lopez-Santiago, L. F., and Isom, L. L. (2019) SCN1B-linked early infantile developmental and epileptic encephalopathy. *Ann. Clin. Transl. Neurol.* **6,** 2354–2367 CrossRef Medline
18. Chen, C., Westenbroek, R. E., Xu, X., Edwards, C. A., Sorenson, D. R., Chen, Y., McEwen, D. P., O'Malley, H. A., Bharucha, V., Meadows, L. S., Knudsen, G. A., Vilaythong, A., Noebels, J. L., Saunders, T. L., Scheuer, T., *et al.* (2004) Mice lacking sodium channel β1 subunits display defects in neuronal excitability, sodium channel expression, and nodal architecture. *J. Neurosci.* **24,** 4030–4042 CrossRef Medline

19. Lin, X., O'Malley, H., Chen, C., Auerbach, D., Foster, M., Shekhar, A., Zhang, M., Coetzee, W., Jalife, J., Fishman, G. I., Isom, L., and Delmar, M. (2015) Scn1b deletion leads to increased tetrodotoxin-sensitive sodium current, altered intracellular calcium homeostasis and arrhythmias in murine hearts. *J. Physiol.* **593,** 1389–1407 CrossRef Medline

20. Lopez-Santiago, L. F., Meadows, L. S., Ernst, S. J., Chen, C., Malhotra, J. D., McEwen, D. P., Speelman, A., Noebels, J. L., Maier, S. K., Lopatin, A. N., and Isom, L. L. (2007) Sodium channel Scn1b null mice exhibit prolonged QT and RR intervals. *J. Mol. Cell. Cardiol.* **43,** 636–647 CrossRef Medline

21. Gray, B., Hasdemir, C., Ingles, J., Aiba, T., Makita, N., Probst, V., Wilde, A. A. M., Newbury-Ecob, R., Sheppard, M. N., Semsarian, C., Sy, R. W., and Behr, E. R. (2018) Lack of genotype-phenotype correlation in Brugada syndrome and sudden arrhythmic death syndrome families with reported pathogenic SCN1B variants. *Heart Rhythm* **15,** 1051–1057 CrossRef Medline

22. Ricci, M. T., Menegon, S., Vatrano, S., Mandrile, G., Cerrato, N., Carvalho, P., De Marchi, M., Gaita, F., Giustetto, C., and Giachino, D. F. (2014) SCN1B gene variants in Brugada syndrome: a study of 145 SCN5A-negative patients. *Sci. Rep.* **4,** 6470 CrossRef Medline

23. Watanabe, H., Koopmann, T. T., Le Scouarnec, S., Yang, T., Ingram, C. R., Schott, J. J., Demolombe, S., Probst, V., Anselme, F., Escande, D., Wiesfeld, A. C., Pfeufer, A., Kaab, S., Wichmann, H. E., Hasdemir, C., *et al.* (2008) Sodium channel β1 subunit mutations associated with Brugada syndrome and cardiac conduction disease in humans. *J. Clin. Invest.* **118,** 2260–2268 CrossRef Medline

24. Watanabe, H., Darbar, D., Kaiser, D. W., Jiramongkolchai, K., Chopra, S., Donahue, B. S., Kannankeril, P. J., and Roden, D. M. (2009) Mutations in sodium channel β1- and β2-subunits associated with atrial fibrillation. *Circ. Arrhythm. Electrophysiol.* **2,** 268–275 CrossRef Medline

25. Olesen, M. S., Holst, A. G., Svendsen, J. H., Haunsø, S., and Tfelt-Hansen, J. (2012) SCN1Bb R214Q found in 3 patients: 1 with Brugada syndrome and 2 with lone atrial fibrillation. *Heart Rhythm* **9,** 770–773 CrossRef Medline

26. Wong, H. K., Sakurai, T., Oyama, F., Kaneko, K., Wada, K., Miyazaki, H., Kurosawa, M., De Strooper, B., Saftig, P., and Nukina, N. (2005) β Subunits of voltage-gated sodium channels are novel substrates of β-site amyloid precursor protein-cleaving enzyme (BACE1) and γ-secretase. *J. Biol. Chem.* **280,** 23009–23017 CrossRef Medline

27. Brigidi, G. S., Sun, Y., Beccano-Kelly, D., Pitman, K., Mobasser, M., Borgland, S. L., Milnerwood, A. J., and Bamji, S. X. (2014) Palmitoylation of δ-catenin by DHHC5 mediates activity-induced synapse plasticity. *Nat. Neurosci.* **17,** 522–532 CrossRef Medline

28. Patino, G. A., Brackenbury, W. J., Bao, Y., Lopez-Santiago, L. F., O'Malley, H. A., Chen, C., Calhoun, J. D., Lafrenière, R. G., Cossette, P., Rouleau, G. A., and Isom, L. L. (2011) Voltage-gated Na$^+$ channel β1B: a secreted cell adhesion molecule involved in human epilepsy. *J. Neurosci.* **31,** 14577–14591 CrossRef Medline

29. Davis, T. H., Chen, C., and Isom, L. L. (2004) Sodium channel β1 subunits promote neurite outgrowth in cerebellar granule neurons. *J. Biol. Chem.* **279,** 51424–51432 CrossRef Medline

30. Haapasalo, A., and Kovacs, D. M. (2011) The many substrates of presenilin/γ-secretase. *J. Alzheimers Dis.* **25,** 3–28 CrossRef Medline

31. Brackenbury, W. J., and Isom, L. L. (2011) Na channel β subunits: overachievers of the ion channel family. *Front. Pharmacol.* **2,** 53 CrossRef Medline

32. Kim, D. Y., Ingano, L. A., Carey, B. W., Pettingell, W. H., and Kovacs, D. M. (2005) Presenilin/γ-secretase–mediated cleavage of the voltage-gated sodium channel β2-subunit regulates cell adhesion and migration. *J. Biol. Chem.* **280,** 23251–23261 CrossRef Medline

33. Bhattacharyya, R., Barren, C., and Kovacs, D. M. (2013) Palmitoylation of amyloid precursor protein regulates amyloidogenic processing in lipid rafts. *J. Neurosci.* **33,** 11169–11183 CrossRef Medline

34. Zhang, S., Wang, Z., Cai, F., Zhang, M., Wu, Y., Zhang, J., and Song, W. (2017) BACE1 cleavage site selection critical for amyloidogenesis and Alzheimer's pathogenesis. *J. Neurosci.* **37,** 6915–6925 CrossRef Medline

35. Cole, S. L., and Vassar, R. (2007) The Alzheimer's disease β-secretase enzyme, BACE1. *Mol. Neurodegener.* **2,** 22 CrossRef Medline

36. Forrester, M. T., Hess, D. T., Thompson, J. W., Hultman, R., Moseley, M. A., Stamler, J. S., and Casey, P. J. (2011) Site-specific analysis of protein *S*-acylation by resin-assisted capture. *J. Lipid Res.* **52,** 393–398 CrossRef Medline

37. Giri, B., Dixit, V. D., Ghosh, M. C., Collins, G. D., Khan, I. U., Madara, K., Weeraratna, A. T., and Taub, D. D. (2007) CXCL12-induced partitioning of flotillin-1 with lipid rafts plays a role in CXCR4 function. *Eur. J. Immunol.* **37,** 2104–2116 CrossRef Medline

38. Percher, A., Ramakrishnan, S., Thinon, E., Yuan, X., Yount, J. S., and Hang, H. C. (2016) Mass-tag labeling reveals site-specific and endogenous levels of protein S-fatty acylation. *Proc. Natl. Acad. Sci. U.S.A.* **113,** 4302–4307 CrossRef Medline

39. Bharadwaj, M., and Bizzozero, O. A. (1995) Myelin P0 glycoprotein and a synthetic peptide containing the palmitoylation site are both autoacylated. *J. Neurochem.* **65,** 1805–1815 CrossRef Medline

40. Kruger, L. C., O'Malley, H. A., Hull, J. M., Kleeman, A., Patino, G. A., and Isom, L. L. (2016) β 1-C121W is down but not out: epilepsy-associated Scn1b-C121W results in a deleterious gain-of-function. *J Neurosci* **36,** 6213–6224 CrossRef Medline

41. Pischedda, F., Szczurkowska, J., Cirnaru, M. D., Giesert, F., Vezzoli, E., Ueffing, M., Sala, C., Francolini, M., Hauck, S. M., Cancedda, L., and Piccoli, G. (2014) A cell surface biotinylation assay to reveal membrane-associated neuronal cues: Negr1 regulates dendritic arborization. *Mol. Cell. Proteomics* **13,** 733–748 CrossRef Medline

42. Levental, I., Lingwood, D., Grzybek, M., Coskun, U., and Simons, K. (2010) Palmitoylation regulates raft affinity for the majority of integral raft proteins. *Proc. Natl. Acad. Sci. U.S.A.* **107,** 22050–22054 CrossRef Medline

43. Noritake, J., Fukata, Y., Iwanaga, T., Hosomi, N., Tsutsumi, R., Matsuda, N., Tani, H., Iwanari, H., Mochizuki, Y., Kodama, T., Matsuura, Y., Bredt, D. S., Hamakubo, T., and Fukata, M. (2009) Mobile DHHC palmitoylating enzyme mediates activity-sensitive synaptic targeting of PSD-95. *J. Cell Biol.* **186,** 147–160 CrossRef Medline

44. Bouza, A. A., Philippe, J. M., Edokobi, N., Pinsky, A. M., Lopez-Santiago, L. F., Offord, J., Jenkins, P. M., and Isom, L. L. (2019) Voltage-gated sodium channel β1 subunit processing by BACE1 and γ-secretase regulates gene transcription. *AES 2019 Annual Meeting Abstract Database*, Abstract 1.022

45. Brigidi, G. S., Santyr, B., Shimell, J., Jovellar, B., and Bamji, S. X. (2015) Activity-regulated trafficking of the palmitoyl-acyl transferase DHHC5. *Nat. Commun.* **6,** 8200 CrossRef Medline

46. Calhoun, J. D., and Isom, L. L. (2014) The role of non−pore-forming β subunits in physiology and pathophysiology of voltage-gated sodium channels. *Handb. Exp. Pharmacol.* **221,** 51–89 CrossRef Medline

47. Patino, G. A., Claes, L. R. F., Lopez-Santiago, L. F., Slat, E. A., Dondeti, R. S. R., Chen, C., O'Malley, H. A., Gray, C. B. B., Miyazaki, H., Nukina, N., Oyama, F., De Jonghe, P., and Isom, L. L. (2009) A functional null mutation of SCN1B in a patient with Dravet syndrome. *J. Neurosci.* **29,** 10764–10778 CrossRef Medline

48. Reverter, M., Rentero, C., de Muga, S. V., Alvarez-Guaita, A., Mulay, V., Cairns, R., Wood, P., Monastyrskaya, K., Pol, A., Tebar, F., Blasi, J., Grewal, T., and Enrich, C. (2011) Cholesterol transport from late endosomes to the Golgi regulates t-SNARE trafficking, assembly, and function. *Mol. Biol. Cell* **22,** 4108–4123 CrossRef Medline

49. Lemaillet, G., Walker, B., and Lambert, S. (2003) Identification of a conserved ankyrin-binding motif in the family of sodium channel alpha subunits. *J. Biol. Chem.* **278,** 27333–27339 CrossRef Medline

50. Srinivasan, Y., Lewallen, M., and Angelides, K. J. (1992) Mapping the binding site on ankyrin for the voltage-dependent sodium channel from brain. *J. Biol. Chem.* **267,** 7483–7489 Medline

51. Xing, D., Wang, J., Ou, S., Wang, Y., Qiu, B., Ding, D., Guo, F., and Gao, Q. (2014) Expression of neonatal Nav1.5 in human brain astrocytoma and its effect on proliferation, invasion and apoptosis of astrocytoma cells. *Oncol. Rep.* **31,** 2692–2700 CrossRef Medline

52. Wang, J., Ou, S. W., Zhang, Z. Y., Qiu, B., and Wang, Y. J. (2018) Molecular expression of multiple Nav1.5 splice variants in the frontal

lobe of the human brain. *Int. J. Mol. Med.* **41,** 915–923 CrossRef Medline

53. Wang, J., Ou, S. W., Bai, Y. F., Wang, Y. J., Xu, Z. D., and Luan, G. M. (2017) Multiple Nav1.5 isoforms are functionally expressed in the brain and present distinct expression patterns compared with cardiac Nav1.5. *Mol. Med. Rep.* **16,** 719–729 CrossRef Medline

54. Abriel, H. (2010) Cardiac sodium channel Na$_v$1.5 and interacting proteins: physiology and pathophysiology. *J. Mol. Cell. Cardiol.* **48,** 2–11 CrossRef Medline

55. El-Husseini, A. E.-D., Schnell, E., Dakoji, S., Sweeney, N., Zhou, Q., Prange, O., Gauthier-Campbell, C., Aguilera-Moreno, A., Nicoll, R. A., and Bredt, D. S. (2002) Synaptic strength regulated by palmitate cycling on PSD-95. *Cell* **108,** 849–863 CrossRef Medline